Design of a Control System using Linear Matrix Inequalities for the Active Vibration Control of a Plate

Samuel Da Silva, Vicente Lopes Junior and Michael J. Brennan

Journal of Intelligent Material Systems and Structures 2006 17: 81
DOI: 10.1177/1045389X06056341

Design of a Control System using Linear Matrix Inequalities for the Active Vibration Control of a Plate

SAMUEL DA SILVA,[1] VICENTE LOPES JÚNIOR[1] AND MICHAEL J. BRENNAN[2,*]

[1]*Grupo de Materiais e Sistemas Inteligentes – GMSINT*
Department of Mechanical Engineering, Universidade Estadual Paulista – UNESP/Ilha Solteira
Av. Brasil, no. 56, ZIP Code, 15385-000, Ilha Solteira – SP, Brazil

[2]*Institute of Sound and Vibration Research, University of Southampton, Southampton, UK*

ABSTRACT: The study of algorithms for active vibration control in smart structures is an area of interest, mainly due to the demand for better performance of mechanical systems, such as aircraft and aerospace structures. Smart structures, formed using actuators and sensors, can improve the dynamic performance with the application of several kinds of controllers. This article describes the application of a technique based on linear matrix inequalities (LMI) to design an active control system. The positioning of the actuators, the design of a robust state feedback controller and the design of an observer are all achieved using LMI. The following are considered in the controller design: limited actuator input, bounded output (energy) and robustness to parametric uncertainties. Active vibration control of a flat plate is chosen as an application example. The model is identified using experimental data by an eigensystem realization algorithm (ERA) and the placement of the two piezoelectric actuators and single sensor is determined using a finite element model (FEM) and an optimization procedure. A robust controller for active damping is designed using an LMI framework, and a reduced model with observation and control spillover effects is implemented using a computer. The simulation results demonstrate the efficacy of the approach, and show that the control system increases the damping in some of the modes.

Key Words: robust control, LMI, active vibration control, smart structures.

INTRODUCTION

VIBRATION reduction is important in many engineering applications, particularly in space vehicles and aircraft. Active vibration control (AVC) in distributed structures is of practical interest because of the demanding requirement for guaranteed performance and stability. This is particularly important in light-weight structures as they generally have low internal damping (Yan and Yam, 2002).

An AVC system requires actuators and sensors and a controller (Clark et al., 1998), and the design process of such a system encompasses three main phases: structural design, optimal placement of sensors and actuators and controller design. For an optimal design, the placement of sensor/actuators on the structure, and the controller have to be considered simultaneously (Lopes et al., 2004).

Two basic approaches, namely open-loop and closed-loop, are normally used for optimal placement of sensors and actuators (Oliveira and Geromel, 2000). The open-loop procedure significantly simplifies the problem because the selection is performed independently of any control law. Practical examples of this procedure are given in Kabamba et al. (1994), Gawronski (1998) and Brasseur et al. (2004). With this approach, however, there is no guarantee that there is the best closed-loop performance. In the closed-loop approach, the goal is to design the controller to minimize some performance criteria, at the same time considering the effects of transducer placement (Geromel, 1989).

There are many robust control techniques described in the literature whose objective is active damping. However, in this article a recent technique involving linear matrix inequalities (LMI) is used, because it has some advantages over conventional controller design approaches. The major advantage is in the design of a controller because it enables many different kinds of constraint to be specified easily, for example stability, decay rate, actuator input limit and a bound on the peak output. In the last decade LMI has been used to solve many problems, not necessarily active vibration control,

*Author to whom correspondence should be addressed.
E-mail: vicente@dem.feis_unesp.br

1045-389X/06/01 00081–14 $10.00/0 DOI: 10.1177/1045389X06056341

which until then were not possible using other methodologies (Boyd et al., 1993, 1994; Grigoriadis and Skelton, 1996). Once formulated in terms of an LMI, a problem can be solved efficiently using convex optimization algorithms, for example, interior-point methods (Gahinet et al., 1995). Limited work has been done on the use of LMI for active vibration control. Sana and Rao (2000) used LMI to design an output feedback controller to increase the damping in some modes of a cantilever beam. However, the resulting matrix inequalities involved bilinear matrix inequalities (BMI) in unknown variables, and hence it became a non-convex optimization problem. Because of this, the BMI could not be solved directly using standard convex optimization software, and it was necessary to use an iterative method, as cone complementary linearization algorithm, described in Ghaoui et al. (1997). Gonçalves et al. (2002) compared H_2 and H_∞ optimal control with state-feedback via LMI of a two degree-of-freedom (2DOF) mechanical system, using a solution procedure proposed by Peres (1997). Gonçalves et al. (2003a, b) designed a state-feedback system using classical LMI as described in Boyd et al. (1994) for a 2DOF mechanical system and a fixed–fixed aluminium beam.

The aim of this article is to illustrate the design procedure of an AVC system using LMI, for parametric uncertainty rejection described by politopic linear differential inclusions (PLDI). A procedure, that was first proposed by Geromel et al. (1991), is used. Active vibration control of a flat plate using two piezoelectric (PZT) actuators and an accelerometer is chosen as an application example. The model is identified using experimental data by an eigensystem realization algorithm (ERA) (Juang and Minh, 2001), and the placement of the two piezoelectric actuators and single sensor is determined using a finite element model (FEM) and an optimization procedure. A robust controller for active damping is designed using an LMI framework, and a reduced model with observation and control spillover effects is implemented using a computer; simulations are presented. Since, not every state is available from measurement, a dynamic observer is also implemented using LMI.

MODAL STATE-SPACE MODEL

A mathematical model of a structure can be obtained by using the finite element method (FEM). Such a model, including the electromechanical coupling between the piezoelectric actuators and the structure, is given by Lopes et al. (2000)

$$\begin{aligned} \mathbf{M}\ddot{\boldsymbol{q}} + \mathbf{D}\dot{\boldsymbol{q}} + \mathbf{K}\boldsymbol{q} &= \mathbf{B}_{\mathrm{T}}\boldsymbol{u} \\ \boldsymbol{y} &= \mathbf{C}_{\boldsymbol{q}}\boldsymbol{q} + \mathbf{C}_{\dot{\boldsymbol{q}}}\dot{\boldsymbol{q}} + \mathbf{C}_{\ddot{\boldsymbol{q}}}\ddot{\boldsymbol{q}} \end{aligned} \qquad (1a, b)$$

where $\mathbf{M}$, $\mathbf{D}$ and $\mathbf{K}$ are the mass, damping and stiffness matrices respectively; $\boldsymbol{q}$ is the displacement vector and the over dot denotes differentiation with respect to time; the matrix $\mathbf{B}_{\mathrm{T}} = [\mathbf{B}_w\ \mathbf{B}_v]$ is a spatial coupling matrix related to the s-length input vector $\boldsymbol{u} = [\boldsymbol{w}\ \boldsymbol{v}]^{\mathrm{T}}$, where $\boldsymbol{w}$ is the disturbance vector and $\boldsymbol{v}$ is the control input vector. The r-length output vector is $\boldsymbol{y}$ which is related to the displacement, velocity and acceleration vectors through the matrices $\mathbf{C}$, $\mathbf{C}_{\dot{\boldsymbol{q}}}$ and $\mathbf{C}_{\ddot{\boldsymbol{q}}}$ respectively.

An example of the coupling matrices for the input control and disturbance vectors are shown in Figure 1(a). Note that in this example only a single actuator is used in each case so the matrices are, in fact, vectors. The PZT elements are driven in anti-phase and thus generate a bending moment. The aim in a placement procedure for a PZT actuator is to find the matrix $\mathbf{B}_v$ that maximizes/minimizes some specified index. A possible configuration for a sensor that measures vertical displacement together with the coupling matrices is shown in Figure 1(b). More

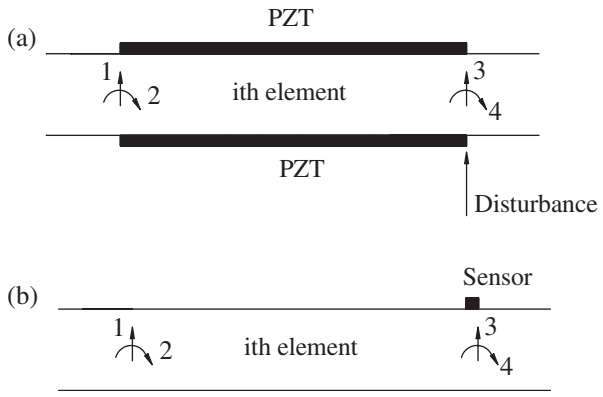

$$\mathbf{B}_w = [\cdots\ 0\ 0\ 1\ 0\ \cdots]^{\mathrm{T}}$$
$$\mathbf{B}_v = [\cdots\ 0\ -1\ 0\ 1\ \cdots]^{\mathrm{T}}$$
$$\mathbf{C}_q = [\cdots\ 0\ 0\ 1\ 0\ \cdots]$$
$$\mathbf{C}_{\dot{q}} = [\cdots\ 0\ 0\ 0\ 0\ \cdots]$$

Figure 1. *Examples of the coupling vectors between the inputs and outputs and the structure. (a) Assembly of the disturbance and control input vectors for a point force and a piezoelectric actuator and (b) assembly of the output vectors for a single displacement sensor.*

information about this topic can be found in Gonçalves et al. (2003b).

Provided that the damping matrix in Equation (1a) can be diagonalized, Equations (1a,b) can be written in modal form as:

$$\begin{aligned} \ddot{\boldsymbol{q}}_m + 2\mathbf{Z}\boldsymbol{\Omega}\dot{\boldsymbol{q}}_m + \boldsymbol{\Omega}^2\boldsymbol{q}_m &= \mathbf{B}_m\boldsymbol{u} \\ \boldsymbol{y} &= \mathbf{C}_{\boldsymbol{q}m}\boldsymbol{q}_m + \mathbf{C}_{\dot{\boldsymbol{q}}m}\dot{\boldsymbol{q}}_m + \mathbf{C}_{\ddot{\boldsymbol{q}}m}\ddot{\boldsymbol{q}}_m \end{aligned} \quad (2a, b)$$

where $\boldsymbol{q}_m = \boldsymbol{\Phi}^{-1}\boldsymbol{q}$ and $\boldsymbol{\Phi}$ is the modal matrix; the $n \times n$ damping matrix is given by $\mathbf{Z} = 0.5(\boldsymbol{\Phi}^{\mathrm{T}}\mathbf{M}\boldsymbol{\Phi})^{-1/2} \times (\boldsymbol{\Phi}^{\mathrm{T}}\mathbf{K}\boldsymbol{\Phi})^{-1/2}(\boldsymbol{\Phi}^{\mathrm{T}}\mathbf{D}\boldsymbol{\Phi})$, the $n \times n$ natural frequency matrix by $\boldsymbol{\Omega} = (\boldsymbol{\Phi}^{\mathrm{T}}\mathbf{M}\boldsymbol{\Phi})^{-1/2}(\boldsymbol{\Phi}^{\mathrm{T}}\mathbf{K}\boldsymbol{\Phi})^{1/2}$, the $n \times s$ modal spatial coupling matrix by $\mathbf{B}_m = (\boldsymbol{\Phi}^{\mathrm{T}}\mathbf{M}\boldsymbol{\Phi})^{-1}\boldsymbol{\Phi}^{\mathrm{T}}\mathbf{B}_{\mathrm{T}}$, the $r \times n$ modal displacement, velocity and acceleration matrices are given by $\mathbf{C}_{\boldsymbol{q}m} = \mathbf{C}_{\boldsymbol{q}}\boldsymbol{\Phi}$, $\mathbf{C}_{\dot{\boldsymbol{q}}m} = \mathbf{C}_{\dot{\boldsymbol{q}}}\boldsymbol{\Phi}$ and $\mathbf{C}_{\ddot{\boldsymbol{q}}m} = \mathbf{C}_{\ddot{\boldsymbol{q}}}\boldsymbol{\Phi}$ respectively. Equations (2a,b) represent a set of n independent equations for each mode of displacement. The equations for the ith mode are given by

$$\begin{aligned} \ddot{\boldsymbol{q}}_{mi} + 2\zeta_i\omega_i\dot{\boldsymbol{q}}_{mi} + \omega_i^2\boldsymbol{q}_{mi} &= \mathbf{B}_{mi}\boldsymbol{u} \\ \boldsymbol{y}_i &= \mathbf{C}_{\boldsymbol{q}mi}\boldsymbol{q}_{mi} + \mathbf{C}_{\dot{\boldsymbol{q}}mi}\dot{\boldsymbol{q}}_{mi} + \mathbf{C}_{\ddot{\boldsymbol{q}}mi}\ddot{\boldsymbol{q}}_{mi} \end{aligned} \quad (3a, b)$$

where $\mathbf{B}_{mi}$ is the ith row of the modal spatial coupling matrix and $\mathbf{C}_{\boldsymbol{q}mi}$, $\mathbf{C}_{\dot{\boldsymbol{q}}mi}$ and $\mathbf{C}_{\ddot{\boldsymbol{q}}mi}$ are the ith columns of the displacement, velocity and acceleration matrices respectively. The modal model, consisting of n modes, can be written in modal state-space form as (Gawronski, 1998),

$$\begin{aligned} \dot{\boldsymbol{x}} &= \mathbf{A}\boldsymbol{x} + \mathbf{B}\boldsymbol{u} \\ \boldsymbol{y} &= \mathbf{C}\boldsymbol{x} + \mathbf{E}\boldsymbol{u} \end{aligned} \quad (4a, b)$$

where the state vector, $\boldsymbol{x}$, in modal coordinates consists of $2n$ independent components, $\boldsymbol{x}_i$, that represents the state of each mode. The ith modal state component is given by

$$\boldsymbol{x}_i = \begin{Bmatrix} \boldsymbol{q}_{mi} \\ \boldsymbol{q}_{moi} \end{Bmatrix},$$

where $\boldsymbol{q}_{moi} = \zeta_i\boldsymbol{q}_{mi} + (\dot{\boldsymbol{q}}_{mi}/\omega_i)$. In Equation (4a) the system matrix is given by the block diagonal matrix $\mathbf{A} = \mathrm{diag}(\mathbf{A}_i)$ where

$$\mathbf{A}_i = \begin{bmatrix} -\zeta_i\omega_i & \omega_i \\ \omega_i\left(\zeta_i^2 - 1\right) & -\zeta_i\omega_i \end{bmatrix}$$

is a 2×2 block, and the spatial coupling matrix is given by the block matrix

$$\mathbf{B} = \begin{bmatrix} \mathbf{B}_1 \\ \mathbf{B}_i \\ \vdots \\ \mathbf{B}_n \end{bmatrix}$$

where

$$\mathbf{B}_i = \begin{bmatrix} 0 \\ \mathbf{B}_{mi} \end{bmatrix}$$

is a $2 \times s$ block. In Equation (4b), $\mathbf{C} = [\mathbf{C}_1\ \mathbf{C}_i\ \ldots\ \mathbf{C}_n]$ is a block matrix, where $\mathbf{C}_i = [\mathrm{C}_{1i}\ \mathbf{C}_{2i}]$ is an $r \times 2$ block, and $\mathbf{C}_{1i} = \mathbf{C}_{\boldsymbol{q}mi} - \omega_i\mathbf{C}_{\dot{\boldsymbol{q}}mi} + \omega_i^2(2\zeta_i^2 - 1)\mathbf{C}_{\ddot{\boldsymbol{q}}mi}$ and $\mathbf{C}_{2i} = \omega_i(\mathbf{C}_{\dot{\boldsymbol{q}}mi} - 2\zeta_i\omega_i\mathbf{C}_{\ddot{\boldsymbol{q}}mi})$; the feedthrough matrix $\mathbf{E}$ is given by $\mathbf{E} = \mathbf{C}_{\ddot{\boldsymbol{q}}m}\mathbf{B}_m$.

PLACEMENT OF SENSORS AND ACTUATORS USING THE H_∞ NORM

The actuators should be placed at points to excite the desired modes most effectively. As mentioned in the introduction there are two approaches to this; open- and closed-loop methods. In this article an open-loop method is used. The controllability Grammian is a good index to use in the choice of actuator positions, however, it is difficult to calculate this index. Recent papers have considered a spatial controllability index using the spatial H_2 norm, for example Halim and Moheimani (2003) and Brasseur et al. (2004). This index maintains the controllability of selected modes without degrading the overall performance of the system. Another approach is to use the H_∞ norm, Gawronski (1998). This approach is adopted here, but the H_∞ norm is determined using LMI. The index quantifies the excitation efficiency of the kth actuator on the ith mode and is defined as

$$\sigma_{ik} = \frac{\|H_{ik}\|_\infty}{\|H\|_\infty}, \quad k = 1, \ldots, R \quad i = 1, \ldots, n \quad (5)$$

where R is the number of candidate actuator positions. The denominator of Equation (5) is the H_∞ norm considering all modes and is chosen so that $0 \le \sigma_{ik} \le 1$. Gonçalves et al. (2002) discuss how to determine this norm by solving a set of LMI and so is only discussed briefly here. The H_∞ norm can be found by solving the following optimization problem

$$\begin{aligned} \|H_{ik}\|_\infty^2 &= \min\ \theta \\ \text{subject to} \quad & \begin{bmatrix} \mathbf{A}_i^{\mathrm{T}}\mathbf{P} + \mathbf{P}\mathbf{A}_i + \mathbf{C}\mathbf{C}^{\mathrm{T}} & \mathbf{P}\mathbf{B}_{\bar{\boldsymbol{v}}k} \\ \mathbf{B}_{\bar{\boldsymbol{v}}k}^{\mathrm{T}}\mathbf{P} & -\theta \end{bmatrix} < 0 \\ & \mathbf{P} > 0 \\ & \theta > 0 \end{aligned} \quad (6)$$

where $\mathbf{P}$ is a symmetric, positive and defined matrix, and θ is the optimization parameter. $\mathbf{A}_i$ is the state matrix of the ith mode and $\mathbf{B}_{\bar{\boldsymbol{v}}k}$ is the part of matrix $\mathbf{B}$ in Equation (4a) that is related to the kth control input. This norm also corresponds to the maximum in the

frequency response function. It is convenient to represent the placement indices as a placement matrix

$$\mathbf{T} = \begin{bmatrix} \sigma_{11} & \sigma_{12} & \cdots & \sigma_{1k} & \cdots & \sigma_{1R} \\ \sigma_{21} & \sigma_{22} & \cdots & \sigma_{2k} & \cdots & \sigma_{2R} \\ \cdots & \cdots & \cdots & \cdots & \cdots & \cdots \\ \sigma_{i1} & \sigma_{i2} & \cdots & \sigma_{ik} & \cdots & \sigma_{iR} \\ \cdots & \cdots & \cdots & \cdots & \cdots & \cdots \\ \sigma_{n1} & \sigma_{n2} & \cdots & \sigma_{nk} & \cdots & \sigma_{nR} \end{bmatrix} \begin{matrix} \\ \\ \\ \Leftarrow i\text{th mode} \\ \\ \\ \Uparrow \\ k\text{th actuator} \end{matrix} \tag{7}$$

where the kth column consists of indices of the kth actuator for each mode, and the ith row is a set of the indices of the ith mode for each actuator. The largest indices indicate optimal actuator placements. It is possible to determine the optimal placement of the sensors in a similar way, as discussed by Gawronski (1998).

Equation (7) can be constructed by varying the matrix $\mathbf{B}_{\bar{\boldsymbol{v}}}$, while fixing $\mathbf{C}$. To simplify matters it is assumed here that the disturbance does not affect the placement of the actuators. If the disturbance is to be considered then it would be necessary to recalculate the index given in Equation (5) including this effect.

STATE-FEEDBACK DESIGN VIA LMI

In this section, a robust controller with a prescribed decay rate and limited output is designed using LMI. The system is described in modal state-space form by Equations (4a, b). The order of the state-space representation is generally very large, causing numerical difficulties. Therefore, the determination of a low-order model is necessary. Equations (4a, b) can be written in terms of controlled (low frequency) modes and residual high frequency modes as

$$\begin{Bmatrix} \dot{\boldsymbol{x}}_\mathrm{c} \\ \dot{\boldsymbol{x}}_\mathrm{r} \end{Bmatrix} = \begin{bmatrix} \mathbf{A}_\mathrm{c}(t) & 0 \\ 0 & \mathbf{A}_\mathrm{r} \end{bmatrix} \begin{Bmatrix} \boldsymbol{x}_\mathrm{c} \\ \boldsymbol{x}_\mathrm{r} \end{Bmatrix} + \begin{bmatrix} \mathbf{B}_\mathrm{c} \\ \mathbf{B}_\mathrm{r} \end{bmatrix} \boldsymbol{u}$$
$$\boldsymbol{y} = \begin{bmatrix} \mathbf{C}_\mathrm{c} & \mathbf{C}_\mathrm{r} \end{bmatrix} \begin{Bmatrix} \boldsymbol{x}_\mathrm{c} \\ \boldsymbol{x}_\mathrm{r} \end{Bmatrix} + \mathbf{E}\boldsymbol{u} \tag{8a, b}$$

where the subscripts $(\cdot)_\mathrm{c}$ and $(\cdot)_\mathrm{r}$ mean controlled and residual modes respectively. The system matrix $\mathbf{A}$ contains parameters which have some uncertainty such that the natural frequencies of the system may change with time. To emphasise this, it is shown as $\mathbf{A}(t)$. It should be noted that the matrix $\mathbf{E}$ is included to allow for an accelerometer to be used as a sensor, which is used in the experimental work in this article. The part of the system matrix $\mathbf{A}_\mathrm{c}(t)$ related to the controlled modes satisfies:

$$\mathbf{A}_\mathrm{c}(t) \in \boldsymbol{\Omega}, \quad \boldsymbol{\Omega} = \mathrm{Co}\{\mathbf{A}_{\mathrm{c},1}, \ldots, \mathbf{A}_{\mathrm{c},v}\} \tag{9}$$

where $\boldsymbol{\Omega}$ is a polytope that is described by a list of vertexes in a convex space Co (Boyd et al., 1994), and v is the number of vertices of the polytopic system. The number of vertices is given by 2^q, where q is the number of parameters that have uncertainty.

The state-feedback control design problem is to determine the state-feedback gain matrix $\mathbf{G}$ in the linear control law $\boldsymbol{v} = \mathbf{G}\boldsymbol{x}_\mathrm{c}$ where $\boldsymbol{v}$ is the vector of control inputs. The part of Equation (8) related to the controlled modes can hence be written as

$$\dot{\boldsymbol{x}}_\mathrm{c} = (\mathbf{A}_\mathrm{c}(t) + \mathbf{B}_{\bar{\boldsymbol{v}}\mathrm{c}}\mathbf{G})\boldsymbol{x}_\mathrm{c}, \quad \mathbf{A}_\mathrm{c}(t) \in \boldsymbol{\Omega} \tag{10}$$

where $\mathbf{B}_{\bar{\boldsymbol{v}}\mathrm{c}}$ is the part of the matrix $\mathbf{B}_\mathrm{c}$ in Equation (8) that is related to the control inputs. The closed-loop system described by Equation (10) is quadratically stable if and only if the following LMI is feasible:

$$\mathbf{Q} > 0, \quad \mathbf{A}_{\mathrm{c},p}\mathbf{Q} + \mathbf{Q}\mathbf{A}_{\mathrm{c},p}^\mathrm{T} + \mathbf{B}_{\bar{\boldsymbol{v}}\mathrm{c}}\mathbf{Y} + \mathbf{Y}^\mathrm{T}\mathbf{B}_{\bar{\boldsymbol{v}}\mathrm{c}}^\mathrm{T} < 0, \quad p = 1, 2, \ldots, v \tag{11}$$

where $\mathbf{Q}$ is a symmetric, positive and defined matrix and $\mathbf{Y} = \mathbf{G}\mathbf{Q}$; both $\mathbf{Y}$ and $\mathbf{Q}$ are regarded as variables. $\mathbf{A}_{\mathrm{c},p}$ is the pth vertex polytopic system, $p = 1, 2, \ldots, v$, where v is the number of vertices (Boyd et al., 1994).

It is assumed that the peak energy of the output is bounded and that $\mathbf{Q}$ satisfies inequality (11). Defining the ellipsoid $\boldsymbol{\varepsilon}$ that is related to the state vector of the controlled modes as (Folcher and Ghaoui, 1994)

$$\boldsymbol{\varepsilon} = \{\boldsymbol{x}_\mathrm{c} \in R^n | \boldsymbol{x}_\mathrm{c}^\mathrm{T}\mathbf{Q}^{-1}\boldsymbol{x}_\mathrm{c} \le 1\} \tag{12}$$

The ellipsoid is said to be invariant if $\boldsymbol{x}_\mathrm{c}(0) \in \boldsymbol{\varepsilon} \Rightarrow \forall t > 0, \quad \boldsymbol{x}_\mathrm{c}(t) \in \boldsymbol{\varepsilon}$, where $\boldsymbol{x}_\mathrm{c}(0)$ is the initial state. The maximum output energy for a given initial state is given by

$$\max\left\{\int_0^\infty \boldsymbol{y}^\mathrm{T}\boldsymbol{y}\,\mathrm{d}t \,\middle|\, \dot{\boldsymbol{x}}_\mathrm{c} = \mathbf{A}_\mathrm{c}(t)\boldsymbol{x}_\mathrm{c},\ \boldsymbol{y} = \mathbf{C}_\mathrm{c}\boldsymbol{x}_\mathrm{c}\right\}, \quad \text{where} \quad \mathbf{A}_\mathrm{c}(t) \in \boldsymbol{\Omega} \tag{13}$$

Suppose there exists a Lyapunov function, $V(\boldsymbol{x}_\mathrm{c}) = \boldsymbol{x}_\mathrm{c}^\mathrm{T}\mathbf{Q}^{-1}\boldsymbol{x}_\mathrm{c}$ such that $\mathbf{Q} > 0$ and $\dot{V}(\boldsymbol{x}) \le -\boldsymbol{y}^\mathrm{T}\boldsymbol{y}$. In an LMI this condition is equivalent to:

$$\mathbf{Q} > 0, \quad \begin{bmatrix} \mathbf{A}_{\mathrm{c},p}\mathbf{Q} + \mathbf{Q}\mathbf{A}_{\mathrm{c},p}^\mathrm{T} & \mathbf{Q}\mathbf{C}_\mathrm{c}^\mathrm{T} \\ \mathbf{C}_\mathrm{c}\mathbf{Q} & -\mathbf{I} \end{bmatrix} \le 0, \quad p = 1, 2, \ldots, v \tag{14}$$

For a given feedback matrix gain $\mathbf{G}$, the output energy of the system does not exceed $V(\boldsymbol{x}_\mathrm{c}) = \boldsymbol{x}_\mathrm{c}^\mathrm{T}\mathbf{Q}^{-1}\boldsymbol{x}_\mathrm{c}$ where $\mathbf{Q}$

satisfies the LMI

$$\begin{bmatrix} \mathbf{A}_{c,p}\mathbf{Q} + \mathbf{Q}\mathbf{A}_{c,p}^{T} + \mathbf{B}_{\bar{\nu}c}\mathbf{Y} + \mathbf{Y}^{T}\mathbf{B}_{\bar{\nu}c}^{T} & (\mathbf{Q}\mathbf{C}_c + \mathbf{E}_{\bar{\nu}}\mathbf{Y})^{T} \\ \mathbf{C}_c\mathbf{Q} + \mathbf{E}_{\bar{\nu}}\mathbf{Y} & -\mathbf{I} \end{bmatrix} \leq 0 \tag{15}$$

where $\mathbf{E}_{\bar{\nu}}$ is the part of matrix $\mathbf{E}$ in Equation (4b), which is related to the control inputs. Regarding $\mathbf{Y}$ as a variable, a state-feedback gain can be found that guarantees output energy to be less than β by solving the LMI problem

$$\begin{bmatrix} \mathbf{Q} & \boldsymbol{x}_c(0) \\ \boldsymbol{x}_c^{T}(0) & \beta \end{bmatrix} > 0 \tag{16}$$

When the initial conditions are known and limited by the conditions given in Equation (12), it is also possible to find an upper bound of the norm of the control input. Given $\mathbf{Q} > 0$ and $\mathbf{Y}$ satisfying the quadratic stabilization condition given by inequality (11), the maximum control input is given by:

$$\begin{aligned} \max_{t \geq 0} \|\boldsymbol{u}\| &= \max_{t \geq 0} \left\|\mathbf{Y}\mathbf{Q}^{-1}\boldsymbol{x}\right\| \leq \max_{\boldsymbol{x} \in \varepsilon} \left\|\mathbf{Y}\mathbf{Q}^{-1}\boldsymbol{x}\right\| \\ &= \lambda_{\max}\left(\mathbf{Q}^{-1/2}\mathbf{Y}^{T}\mathbf{Y}\mathbf{Q}^{-1/2}\right) \end{aligned} \tag{17}$$

where $\lambda_{\max}\left(\mathbf{Q}^{-1/2}\mathbf{Y}^{T}\mathbf{Y}\mathbf{Q}^{-1/2}\right)$ is the maximum eigenvalue. Therefore, the constraint is enforced for $t \geq 0$ provided that the LMI below holds

$$\begin{bmatrix} 1 & \boldsymbol{x}_c(0)^{T} \\ \boldsymbol{x}_c(0) & \mathbf{Q} \end{bmatrix} \geq 0, \quad \begin{bmatrix} \mathbf{Q} & \mathbf{Y}^{T} \\ \mathbf{Y} & \mu^2\mathbf{I} \end{bmatrix} > 0 \tag{18}$$

where μ is the maximum value of the control amplitude. In the same way, it is possible to impose a decay rate, α, on the closed-loop

$$\begin{aligned} &\mathbf{Q} > 0, \quad 2\alpha\mathbf{Q} + \mathbf{A}_{c,p}\mathbf{Q} + \mathbf{Q}\mathbf{A}_{c,p}^{T} + \mathbf{B}_{\bar{\nu}c}\mathbf{Y} + \mathbf{Y}^{T}\mathbf{B}_{\bar{\nu}c}^{T} < 0, \\ &\qquad p = 1, 2, \ldots, v \end{aligned} \tag{19}$$

In summary, the controller design is the result of the following LMI problem, where α, μ and β are known

$$\begin{aligned} &\begin{bmatrix} \begin{pmatrix} \mathbf{A}_{c,p}\mathbf{Q} + \mathbf{Q}\mathbf{A}_{c,p}^{T} \\ + \mathbf{B}_{\bar{\nu}c}\mathbf{Y} + \mathbf{Y}^{T}\mathbf{B}_{\bar{\nu}c}^{T} \end{pmatrix} & (\mathbf{C}_c\mathbf{Q} + \mathbf{E}_{\bar{\nu}}\mathbf{Y})^{T} \\ \mathbf{C}_c\mathbf{Q} + \mathbf{E}_{\bar{\nu}}\mathbf{Y} & -\mathbf{I} \end{bmatrix} \leq 0 \\ &\begin{bmatrix} \mathbf{Q} & \boldsymbol{x}_c(0) \\ \boldsymbol{x}_c^{T}(0) & \beta \end{bmatrix} > 0 \\ &\begin{bmatrix} 1 & \boldsymbol{x}_c(0)^{T} \\ \boldsymbol{x}_c(0) & \mathbf{Q} \end{bmatrix} \geq 0 \qquad p = 1, 2, \ldots, v \\ &\begin{bmatrix} \mathbf{Q} & \mathbf{Y}^{T} \\ \mathbf{Y} & \mu^2\mathbf{I} \end{bmatrix} > 0 \\ &\mathbf{Q} > 0 \\ &2\alpha\mathbf{Q} + \mathbf{A}_{c,p}\mathbf{Q} + \mathbf{Q}\mathbf{A}_{c,p}^{T} + \mathbf{B}_{\bar{\nu}c}\mathbf{Y} + \mathbf{Y}^{T}\mathbf{B}_{\bar{\nu}c}^{T} < 0 \end{aligned} \tag{20}$$

The resulting controller feedback gain is given by

$$\mathbf{G} = \mathbf{Y}\mathbf{Q}^{-1} \tag{21}$$

where $\mathbf{Y}$ and $\mathbf{Q}$ are the solution such that LMI problem given by Equation (20) is feasible. For each initial condition, the input $\boldsymbol{u}$ and the output $\boldsymbol{y}$ are such that

$$\forall t \geq 0, \quad \begin{cases} \|\boldsymbol{u}\| < \mu e^{-\alpha t} \\ \|\boldsymbol{y}\| < \beta e^{-\alpha t} \end{cases} \tag{22}$$

The matrices $\mathbf{Y}$ and $\mathbf{Q}$ are not unique; the solutions are feasible, not optimal. However, it is also possible to define a variable of optimization, as for instance, the decay rate α and to solve a generalized eigenvalue problem (Boyd et al., 1994). In that case, the matrices, $\mathbf{Y}$ and $\mathbf{Q}$ would correspond to the optimal solution and would be unique.

Dynamic Observer Via LMI

Some states are not always available for feedback control, since a limited number of sensors are available, or it can have state variables that are difficult to access, or they are not measurable directly. In these cases, it is essential to design observers and this is the subject of this section. The control input is given by

$$\boldsymbol{v} = \mathbf{G}\bar{\boldsymbol{x}}_c \tag{23}$$

where $\bar{\boldsymbol{x}}_c$ is the modal state vector to be observed. The linear equation of the modal observer can be written as (Meirovitch, 1990):

$$\dot{\bar{\boldsymbol{x}}}_c = \mathbf{A}_c(t)\bar{\boldsymbol{x}}_c + \mathbf{B}_{\bar{\nu}c}\mathbf{G}\bar{\boldsymbol{x}}_c + \mathbf{B}_{\bar{w}c}\boldsymbol{w} + \mathbf{L}(\mathbf{C}_c\bar{\boldsymbol{x}}_c + \mathbf{E}_{\bar{\nu}}\mathbf{G}\bar{\boldsymbol{x}}_c - \boldsymbol{y}) \tag{24}$$

where $\mathbf{B}_{\bar{w}c}$ is the part of the matrix $\mathbf{B}_c$ in Equation (8) that is related to the disturbance, and $\mathbf{L}$ is the observer gain matrix, which can be determined using LMI. It is possible to find an observer gain through the solution of the following (Boyd et al., 1994):

$$\begin{aligned} &\mathbf{P} > 0, \quad 2\gamma\mathbf{P} + \mathbf{A}_{c,p}^{T}\mathbf{P} + \mathbf{P}\mathbf{A}_{c,p} + \mathbf{W}\mathbf{C}_c + \mathbf{C}_c^{T}\mathbf{W}^{T} < 0, \\ &\qquad p = 1, 2, \ldots, v \end{aligned} \tag{25}$$

where γ is the decay rate of the observer, with $\gamma \gg \alpha$. For every $\mathbf{P}$ and $\mathbf{W}$ satisfying these LMI, there corresponds a stabilizing observer. The inequality (25) is very similar to inequality (11). The observer gain is given by:

$$\mathbf{L} = \mathbf{P}^{-1}\mathbf{W} \tag{26}$$

where $\mathbf{P}$ and $\mathbf{W}$ are solutions from LMI problem given in Equation (25). Equation (26) is very similar to Equation (21) that corresponds to the gain matrix of the

controller. However, the sensor signals include contributions from controlled and residual modes, so the output vector is (Meirovitch, 1990)

$$\boldsymbol{y} = \mathbf{C}_{\mathrm{c}}\boldsymbol{x}_{\mathrm{c}} + \mathbf{C}_{\mathrm{r}}\boldsymbol{x}_{\mathrm{r}} + \mathbf{E}_{\bar{\boldsymbol{v}}}\mathbf{G}\bar{\boldsymbol{x}}_{\mathrm{c}} \tag{27}$$

Substituting into Equation (24) gives

$$\dot{\bar{\boldsymbol{x}}}_{\mathrm{c}} = \mathbf{A}_{\mathrm{c}}(t)\,\bar{\boldsymbol{x}}_{\mathrm{c}} + \mathbf{B}_{\bar{\boldsymbol{v}}\mathrm{c}}\mathbf{G}\bar{\boldsymbol{x}}_{\mathrm{c}} + \mathbf{B}_{\bar{\boldsymbol{w}}\mathrm{c}}\boldsymbol{w} + \mathbf{L}\mathbf{C}_{\mathrm{c}}(\bar{\boldsymbol{x}}_{\mathrm{c}} - \boldsymbol{x}_{\mathrm{c}}) - \mathbf{L}\mathbf{C}_{\mathrm{r}}\boldsymbol{x}_{\mathrm{r}} \tag{28}$$

Considering a polytopic system for the low frequency modes, and substituting into Equation (8) gives

$$\begin{aligned} \dot{\boldsymbol{x}}_{\mathrm{c}} &= \mathbf{A}_{\mathrm{c}}(t)\boldsymbol{x}_{\mathrm{c}} + \mathbf{B}_{\bar{\boldsymbol{v}}\mathrm{c}}\mathbf{G}\bar{\boldsymbol{x}}_{\mathrm{c}} \\ \dot{\boldsymbol{x}}_{\mathrm{r}} &= \mathbf{A}_{\mathrm{r}}\boldsymbol{x}_{\mathrm{r}} + \mathbf{B}_{\bar{\boldsymbol{v}}\mathrm{r}}\mathbf{G}\bar{\boldsymbol{x}}_{\mathrm{c}} \end{aligned} \tag{29a, b}$$

The error vector can be written as:

$$\dot{\boldsymbol{e}}_{\mathrm{c}} = (\mathbf{A}_{\mathrm{c}}(t) + \mathbf{L}\mathbf{C}_{\mathrm{c}})\boldsymbol{e}_{\mathrm{c}} - \mathbf{L}\mathbf{C}_{\mathrm{r}}\boldsymbol{x}_{\mathrm{r}} \quad \text{where } \boldsymbol{e}_{\mathrm{c}} = \bar{\boldsymbol{x}}_{\mathrm{c}} - \boldsymbol{x}_{\mathrm{c}} \tag{30}$$

Equations (29) can be rearranged and written in matrix form as

$$\begin{Bmatrix} \dot{\boldsymbol{x}}_{\mathrm{c}} \\ \dot{\boldsymbol{x}}_{\mathrm{r}} \\ \dot{\boldsymbol{e}}_{\mathrm{c}} \end{Bmatrix} = \begin{bmatrix} \mathbf{A}_{\mathrm{c}}(t) + \mathbf{B}_{\bar{\boldsymbol{v}}\mathrm{c}}\mathbf{G} & 0 & \mathbf{B}_{\bar{\boldsymbol{v}}\mathrm{c}}\mathbf{G} \\ \mathbf{B}_{\bar{\boldsymbol{v}}\mathrm{r}}\mathbf{G} & \mathbf{A}_{\mathrm{r}} & \mathbf{B}_{\bar{\boldsymbol{v}}\mathrm{r}}\mathbf{G} \\ 0 & -\mathbf{L}\mathbf{C}_{\mathrm{r}} & \mathbf{A}_{\mathrm{c}}(t) + \mathbf{L}\mathbf{C}_{\mathrm{c}} \end{bmatrix} \begin{Bmatrix} \boldsymbol{x}_{\mathrm{c}} \\ \boldsymbol{x}_{\mathrm{r}} \\ \boldsymbol{e}_{\mathrm{c}} \end{Bmatrix} \tag{31}$$

The term $\mathbf{B}_{\bar{\boldsymbol{v}}\mathrm{r}}\mathbf{G}$ is responsible for the excitation of residual modes by the control forces which is known as *control spillover*. This term has no effect on the eigenvalues of the closed-loop system and it cannot destabilize the system, although it can cause some degradation in the performance. However, the term $-\mathbf{L}\mathbf{C}_{\mathrm{r}}$ can produce instability in the residual modes. This effect is known as *observation spillover*. However, a small amount of modal damping, inherent in the structure, is often sufficient to overcome the observation spillover effect. Another way to reduce this effect is to use a large number of sensors or to filter the sensor signals, in order to screen out the contribution of residual modes (Meirovitch, 1990). Other methods to suppress spillover effects can be found in Charon (1997).

APPLICATION EXAMPLE

To verify the proposed methodology, an aluminum plate structure shown in Figure 2, with dimensions given in Table 1, was considered. The structure was modeled using FEM, with 10×10 elements, each with 4 nodes and 3 degrees of freedom (dof) per node (one vertical displacement, one rotation in x and one rotation in y). The boundary conditions were clamped-free-free-free. To verify the proposed placement methodology, the first step was to find the placement of two pairs of PZT elements, bonded on both sides of the plate surface, using the FEM model. The PZT elements generate moments at their edges (out-of-phase). The number of electrical dof changes as a function of the number of piezoelectric elements considered (2 dof per PZT) (Lopes et al., 2004). The properties of the PZT elements used are shown in Table 2. Figure 2(a) shows the discretization of the plate, where the numbers 1 to 11 . . . 121, indicate the nodes of the model. It was considered that each PZT actuator could be positioned at these nodes. In practice, some physical constraints could be imposed to reduce the number of candidate actuator positions, for example, it was not considered practical to fix the PZT elements to the first row (clamped edge). So, in

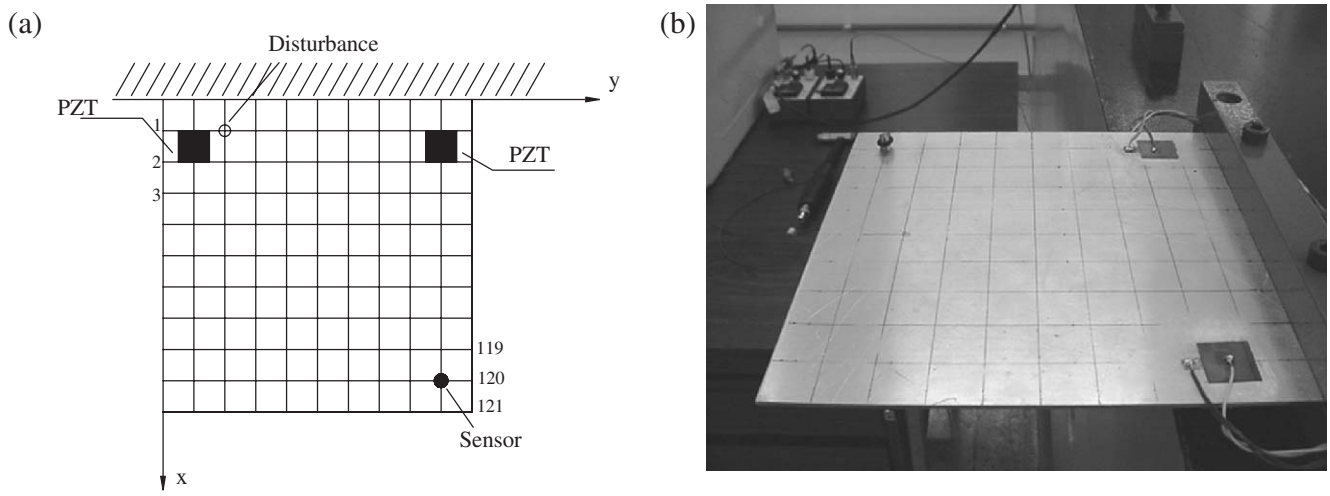

Figure 2. *(a) Schematic structure and (b) view of the setup with the flat plate, accelerometer and PZT actuators.*

Table 1. Properties of host structure.

Property	Value
Length	0.2 m
Width	0.2 m
Thickness	0.002 m
Young's modulus	70 GPa
Density	2710 kg m^{-3}

Table 2. Properties of PZT, based on material designation PSI-5A-S4 (Piezo Systems®, Inc.).

Property	Value
Length	0.02 m
Width	0.02 m
Thickness	0.00027 m
Young's modulus	60 GPa
Density	7650 kg m^{-3}
Dielectric constant	190e−12 m V^{-1}
Dielectric permittivity	30.705 C/m^2
Elasticity	1.076e−11 m/N^2
Permittivity of space	7.33e−9 F/m

this example, 99 candidate locations for the PZT elements were considered. Figure 2(b) shows a view of the setup.

The placement indices of each candidate actuator for the first and second modes are shown in Figure 3 (these correspond the two first lines of matrix **T** from Equation (7)). As can be seen in Figure 3, the results are symmetric. The largest index for the actuator position corresponds to the best location to control the two first modes. These figures were constructed by varying $\mathbf{B}_v$ in Equation (1) (maintaining the output fixed) and obtaining the modal reduced state-space model, based on the FEM model. Finally, the H_∞ norm was found by solving the LMI in Equation (6), considering only the two first modes. One pair of PZT actuators was chosen to attenuate the first mode, while the second pair was chosen to attenuate the second mode of vibration. Figure 4 shows the experimental setup and the position of the PZT actuators and the sensor. The position of the disturbance input is shown in Figure 2(a). The procedure to choose the best position for the sensor was similar to that for the actuators.

To obtain the dynamic characteristics of the system for use in control design and simulations, some tests were performed. The system was excited separately by impact hammer (disturbance input), and by the two pairs of PZT actuators (control input). Because of symmetry, the two pairs of PZT actuators were considered as a single unit and the input voltage was applied to both at the same time. The output (signal for feedback) was measured with an accelerometer, PCB Piezotronics® model 352A10, and the resulting

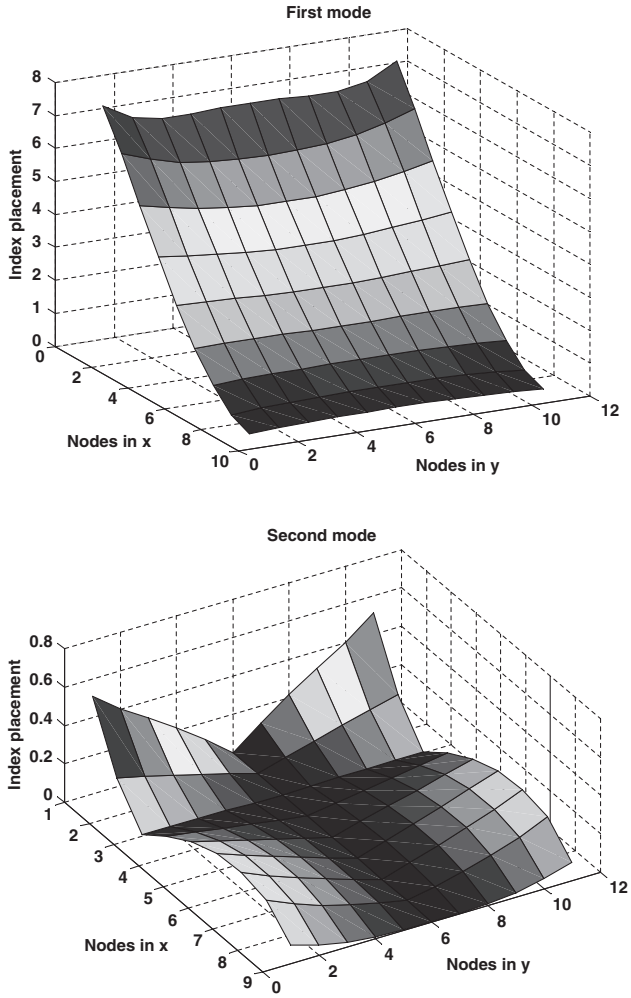

Figure 3. *Placement indexes of PZT actuator for first and second modes, respectively, vs PZT location.*

frequency response functions (FRFs) had a frequency resolution of 1.25 Hz. In this experiment the software SignalCalc ACE® was used to generate a swept sine signal (bandwidth 0–1000 Hz) for the PZT and to do the data acquisition. The impact hammer used was a PCB Piezotronics® model 086C04. Once the data was collected, a model of the system had to be determined from the experimental data. A ten-mode model was identified using an ERA (Juang and Minh, 2001). In fact, the real system has nine modes in the frequency range of interest, but ERA adds a highly damped computation mode to the model. The natural frequencies obtained experimentally and by the FEM are listed in Table 3.

The FRFs of the real system and of the identified model are shown in Figures 5(a) and 6(a), for excitation with an inpact hammer and PZT actuators, respectively. A fourth model is obtained by truncating the model. The FRF amplitude plots H_1 and H_2 for reduced and residual models are shown in Figures 5(b) and 6(b) respectively.

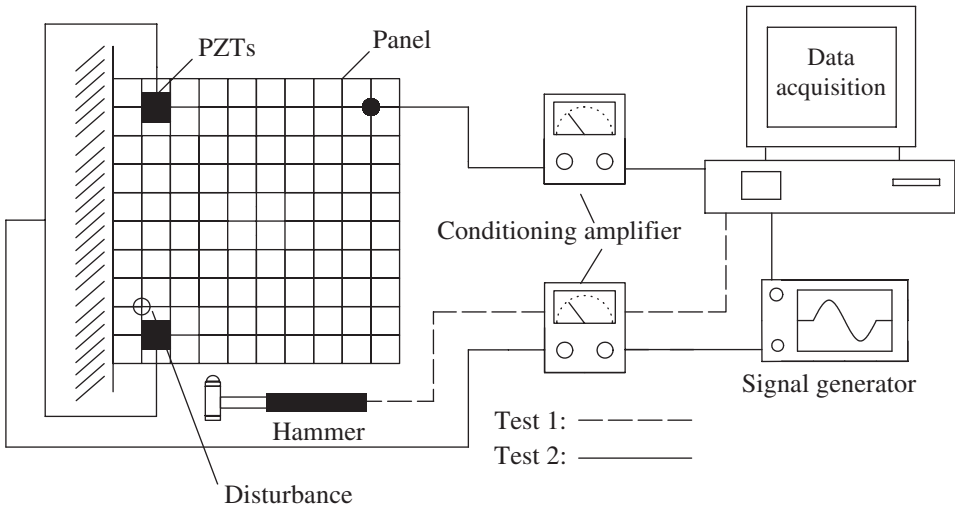

Figure 4. *Schematic diagram of the measurement setup to identify the model.*

Table 3. Evaluated natural frequencies (Hz).

Mode	FEM	Experimental	% Difference
1	43.00	43.22	0.5
2	104.00	102.09	1.8
3	261.56	259.15	0.9
4	332.42	340.36	2.3
5	379.03	373.06	1.6
6	659.7	660.61	0.2
7	750.8	745.00	0.8
8	785.51	796.22	1.3
9	867.23	861.19	0.7

Since no single fixed model can respond exactly like the true system, uncertainties need to be accounted for in the system. The parameter uncertainty ranges can be described as a parameter box. The controller that satisfies all systems described inside this convex space is said to be robust to parametric variations. It is enough to solve the LMI problem in Equation (20), for the controller, and Equation (25), for the observer, for all vertices of the system simultaneously. In the example considered here, it was assumed that the system could have a possible variation in the first and second natural frequencies of ±15%, giving two uncertainty parameters

$$\omega_1 \in \left[\omega_1^{\min} = 0.85\omega_1 \quad \omega_1^{\max} = 1.15\omega_1\right]$$

$$\omega_2 \in \left[\omega_2^{\min} = 0.85\omega_2 \quad \omega_2^{\max} = 1.15\omega_2\right]$$

where ω_i is ith natural frequency in a nominal condition (measured in the experiments described earlier). These uncertainties are shown in Figure 7. The vertices of the parameter box are combinations of the minimum and maximum values of the parameters of the system. It is assumed that the system can have any combination of values inside the box. The system matrix for the four vertices is given by

$$\mathbf{A}_{c,1} = \begin{bmatrix} -\zeta_1\omega_1^{\min} & \omega_1^{\min} & 0 & 0 \\ \omega_1^{\min}\left(\zeta_1^2-1\right) & -\zeta_1\omega_1^{\min} & 0 & 0 \\ 0 & 0 & -\zeta_2\omega_2^{\min} & \omega_2^{\min} \\ 0 & 0 & \omega_2^{\min}\left(\zeta_2^2-1\right) & -\zeta_2\omega_2^{\min} \end{bmatrix}$$

$\Rightarrow$ vertex V1

$$\mathbf{A}_{c,2} = \begin{bmatrix} -\zeta_1\omega_1^{\max} & \omega_1^{\max} & 0 & 0 \\ \omega_1^{\max}\left(\zeta_1^2-1\right) & -\zeta_1\omega_1^{\max} & 0 & 0 \\ 0 & 0 & -\zeta_2\omega_2^{\min} & \omega_2^{\min} \\ 0 & 0 & \omega_2^{\min}\left(\zeta_2^2-1\right) & -\zeta_2\omega_2^{\min} \end{bmatrix}$$

$\Rightarrow$ vertex V2

$$\mathbf{A}_{c,3} = \begin{bmatrix} -\zeta_1\omega_1^{\min} & \omega_1^{\min} & 0 & 0 \\ \omega_1^{\min}\left(\zeta_1^2-1\right) & -\zeta_1\omega_1^{\min} & 0 & 0 \\ 0 & 0 & -\zeta_2\omega_2^{\max} & \omega_2^{\max} \\ 0 & 0 & \omega_2^{\max}\left(\zeta_2^2-1\right) & -\zeta_2\omega_2^{\max} \end{bmatrix}$$

$\Rightarrow$ vertex V3

$$\mathbf{A}_{c,4} = \begin{bmatrix} -\zeta_1\omega_1^{\max} & \omega_1^{\max} & 0 & 0 \\ \omega_1^{\max}\left(\zeta_1^2-1\right) & -\zeta_1\omega_1^{\max} & 0 & 0 \\ 0 & 0 & -\zeta_2\omega_2^{\max} & \omega_2^{\max} \\ 0 & 0 & \omega_2^{\max}\left(\zeta_2^2-1\right) & -\zeta_2\omega_2^{\max} \end{bmatrix}$$

$\Rightarrow$ vertex V4

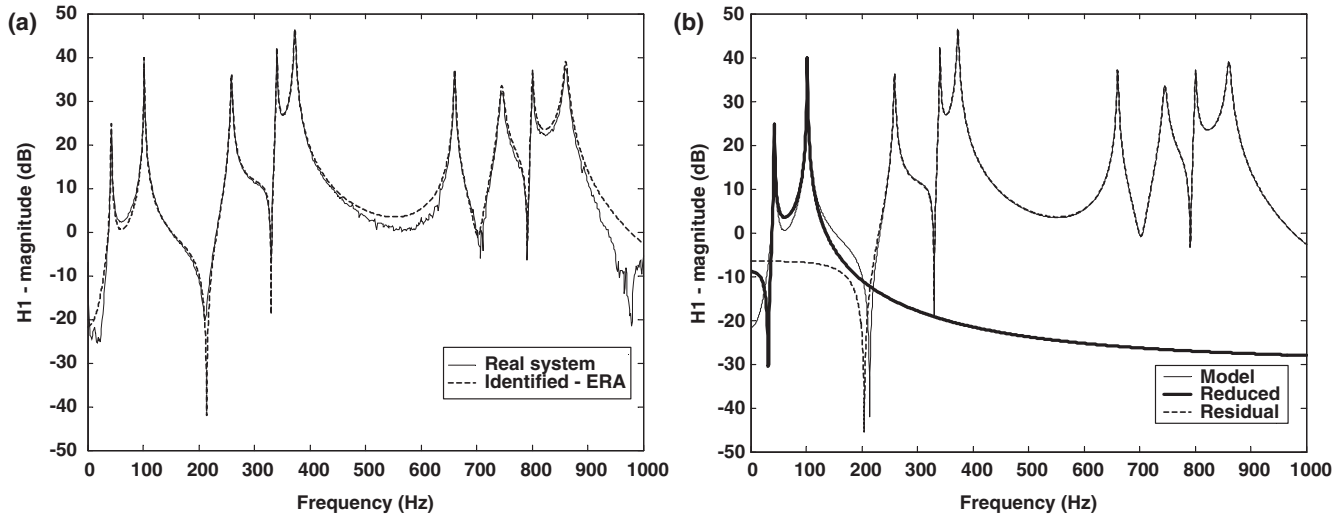

Figure 5. *FRF of the plate structure excited by impact hammer. H_1 is related with $(\boldsymbol{A}, \boldsymbol{B}_{\bar{w}}, \boldsymbol{C}, \boldsymbol{E}_{\bar{w}})$ where $\boldsymbol{A}$ is the system matrix, $\boldsymbol{B}_{\bar{w}}$ is the disturbance input matrix, $\boldsymbol{C}$ is the output matrix, and $\boldsymbol{E}_{\bar{w}}$ is the direct-transmission term from the disturbance input to output signal. (a) Real system vs identified model by ERA and (b) complete, reduced and residual models.*

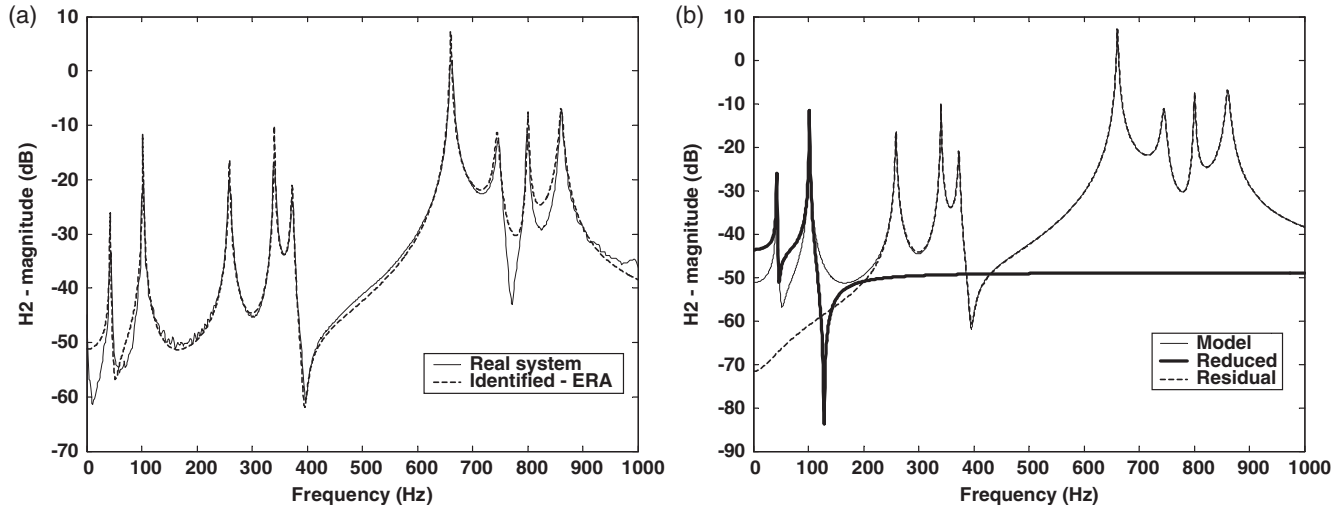

Figure 6. *FRF of the plate structure excited by PZTs actuators. H_2 is related with $(\boldsymbol{A}, \boldsymbol{B}_{\bar{v}}, \boldsymbol{C}, \boldsymbol{E}_{\bar{v}})$, where $\boldsymbol{A}$ is the dynamic matrix, $\boldsymbol{B}_{\bar{v}}$ is the control input matrix, $\boldsymbol{C}$ is the output matrix, and $\boldsymbol{E}_{\bar{v}}$ is the direct-transmission term from the control input to output signal. (a) Real system vs identified model by ERA and (b) complete, reduced and residual models.*

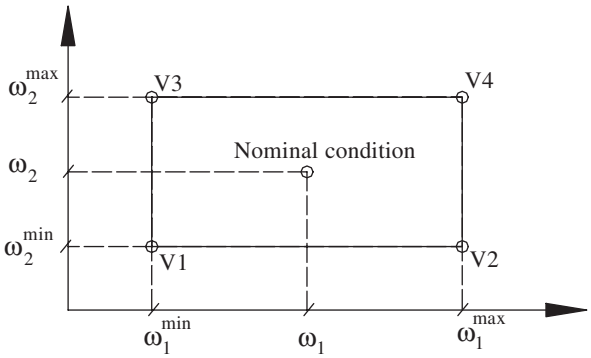

Figure 7. *Parameter box showing the uncertainty combinations for the first two natural frequencies.*

and the variation in the FRFs is illustrated in Figure 8.

The object of the controller is to increase the damping of the first two modes. This is achieved from the solution of the LMI problems of Equations (20) and (25), with $\boldsymbol{x}_c(0) = \begin{bmatrix} -0.01 & 0 & -0.01 & 0 \end{bmatrix}^T$, which represents an initial modal displacement of -0.01 m in the first two modes, $\alpha = 5$, $\gamma = 15$, $\mu = 10$ and $\beta = 2$.

Figure 9 compares the FRF magnitude plots of the uncontrolled and controlled system, for the H_1 transfer function. Table 4 shows the attenuation achieved in the first nine modes by the active control system, comparing the system in its uncontrolled and

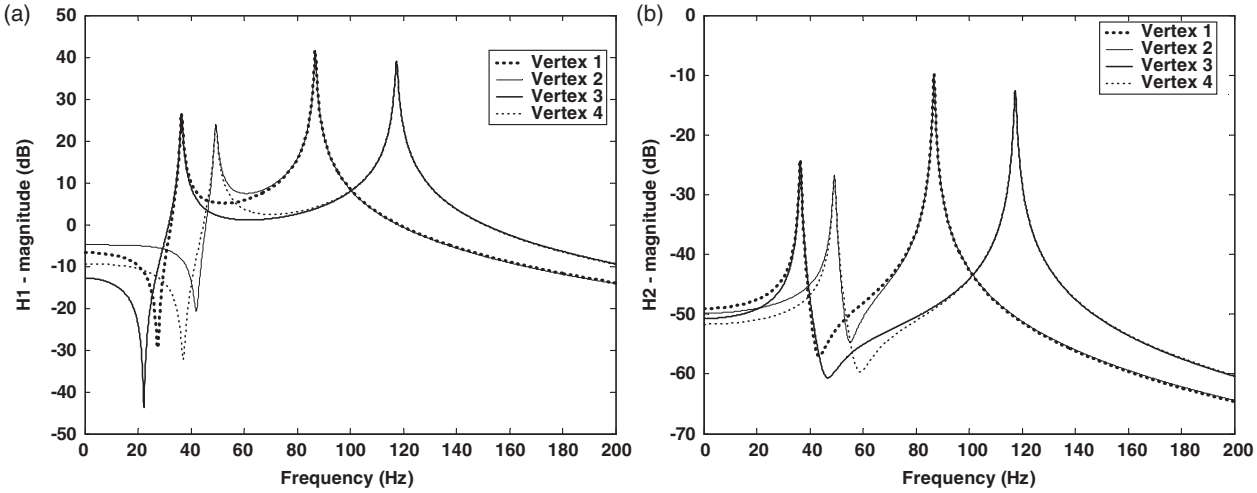

Figure 8. *Magnitude plots of the two first modes for all four vertices situation (parametric variation). (a) System excited by impact hammer and (b) system excited by PZTs actuators.*

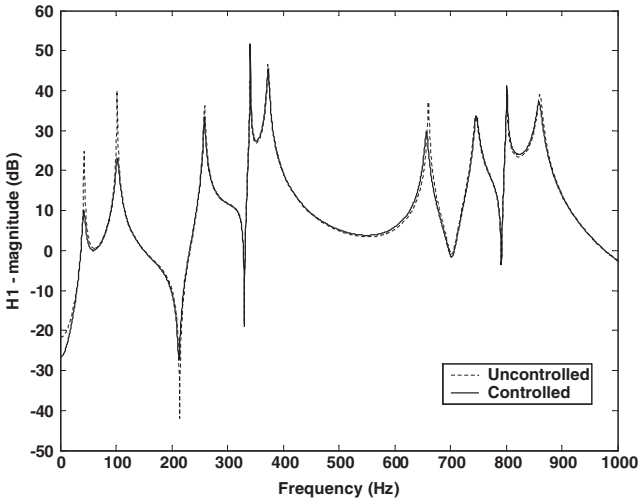

Figure 9. *H_1 FRF for uncontrolled and controlled system in the nominal condition – simulated system by computer.*

Table 4. Control performance in nominal condition.

	Uncontrolled		Controlled		Attenuation
Mode	Mag. (dB)	Damping ratio	Mag. (dB)	Damping ratio	Mag. (dB)
1	25.1	0.0101	9.9	0.053	−15.2
2	40.1	0.0037	22.8	0.024	−17.3
3	36.5	0.0041	33.1	0.0058	−3.4
4	42.3	0.0019	51.2	0.00045	+8.9
5	46.3	0.0038	45.4	0.0044	−0.9
6	36.8	0.0017	29.8	0.004	−7.0
7	33.4	0.00458	33.4	0.0044	0.0
8	36.5	0.00148	41.4	0.000977	+4.9
9	39.0	0.00384	37.0	0.00503	−2.0

controlled state. As a result of the active damping, the peaks at the resonance frequencies of the controlled modes are reduced. Furthermore, the amplitudes of some of the other modes, which are not explicitly included in the controller, are also reduced, for example, the amplitudes at modes 3 and 6 have been attenuated by 3.4 and 7.0 dB, respectively. Nevertheless, some peaks have increased, for example, the amplitudes at modes 4 and 8 have increased by 9.0 and 4.3 dB, respectively. This occurred, because of *control spillover*.

Figure 10 shows the response in time domain for uncontrolled and controlled system and some residual modes, considering −0.01 m of modal displacement as initial condition in the first two modes. Only the first two graphs in Figure 11 show the response for uncontrolled as well as the controlled system. A negligible influence of the high frequency dynamics on the structural control performance is observed. Comparing the modal amplitude of the residual modes in this figure, it can be observed that spillover effects exist, but these are small when compared with the modal amplitudes of the controlled modes.

To test the robustness of the controller to parametric variation, the system was simulated in extreme conditions. Figure 11 shows the FRFs of the controlled and uncontrolled structures for the four vertices of the polytopic system, representing the parametric variation caused by uncertainties in natural frequencies. Good control of the first two modes is achieved in all cases.

CONCLUSIONS

The main contribution of this work is to demonstrate the design of an active vibration control system using LMI. The positioning of the actuators, the design of a state feedback controller robust to polytopic uncertainties and the design of an observer have all been achieved using LMI. To illustrate this procedure the control of a plate was considered using piezoelectric actuators and an accelerometer. The model was

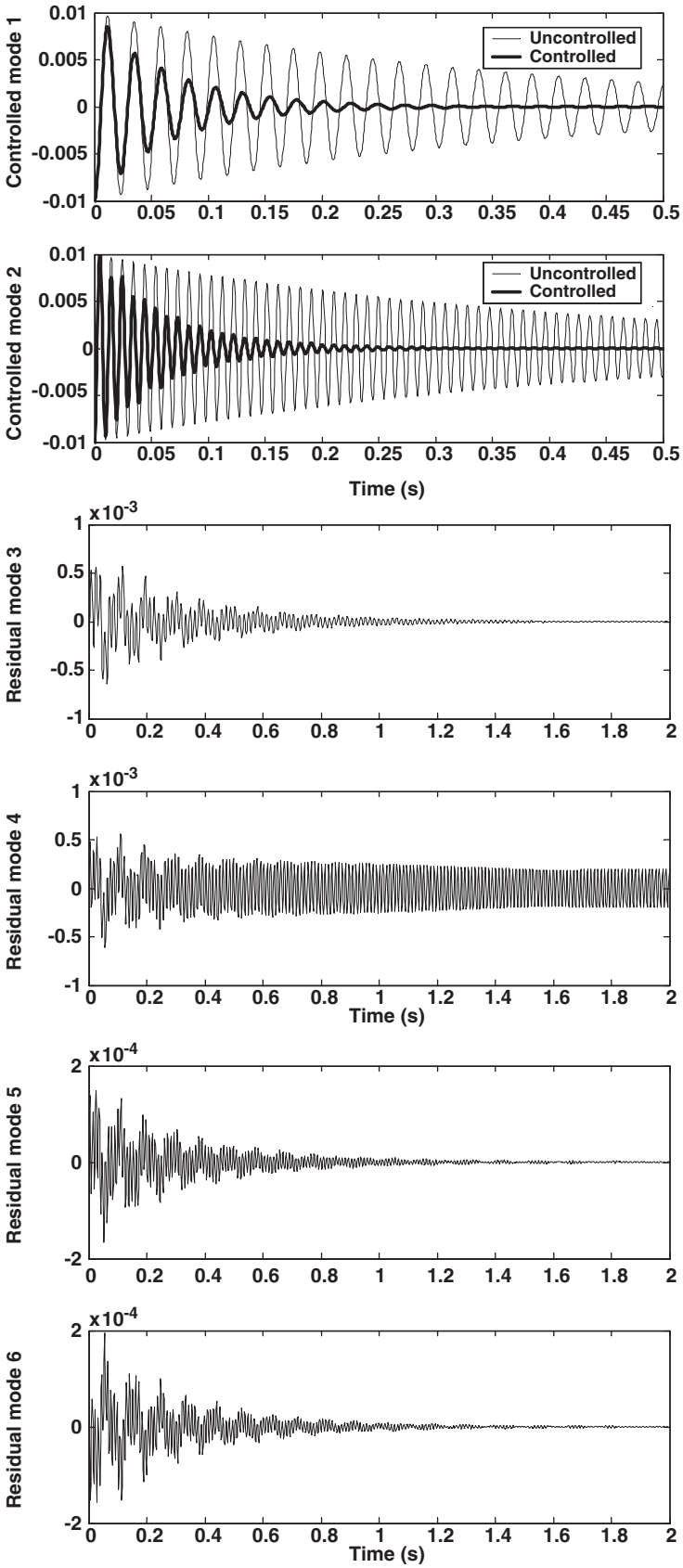

Figure 10. *Time domain response for open-loop and closed-loop for the first two modes, considering the system in the nominal condition, disturbance in residual modes caused by input control excitation.*

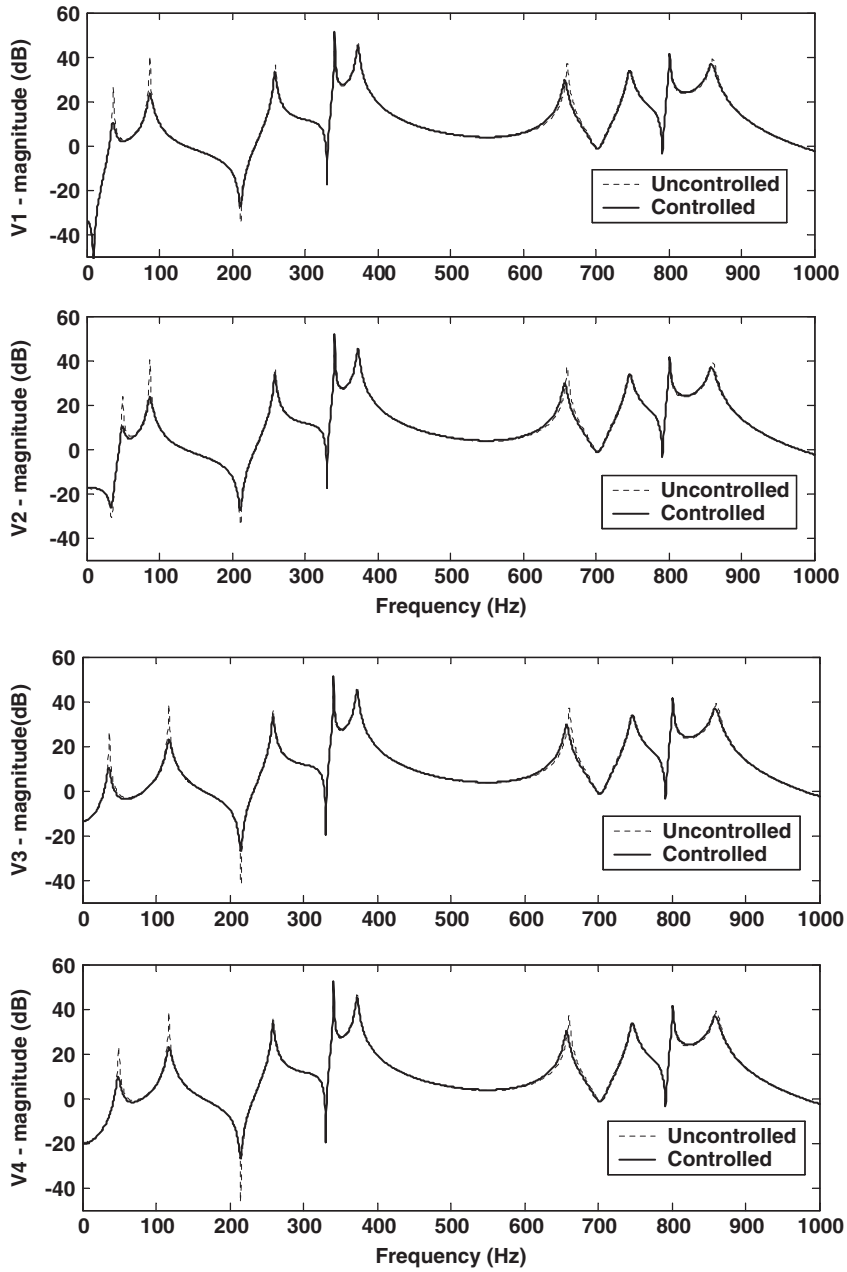

Figure 11. *FRF for uncontrolled and controlled system considering parametric variations, for the system in condition of vertices, H_1 transfer function amplitude.*

obtained from experimental data, and simulations showed that the first two modes could be significantly attenuated even when their natural frequencies changed by up to ±15%.

ACKNOWLEDGMENTS

The first author was supported by a scholarship from Research Foundation of the State of São Paulo (FAPESP-Brazil). This work was possible due to the cooperative agreement between UNESP/Ilha Solteira, Brazil, and the Institute of Sound and Vibration Research, University of Southampton, UK, with financial support from CNPq/Brazil and British Council.

REFERENCES

Boyd, S., Balakrishnan, V., Feron, E. and El Ghaoui, L. 1993. "Control System Analysis and Synthesis via Linear Matrix Inequalities," In: *Proceeding of American Control Conference*, 2:2147–2154.

Boyd, S., Balakrishnan, V., Feron, E. and El Ghaoui, L. 1994. *Linear Matrix Inequalities in Systems and Control Theory*, p. 193, SIAM Studies in Applied Mathematics, USA.

Brasseur, M., De Boe, P., Golinval, J.C., Tamaz, P., Caule, P., Embrechts, J.-J. and Nemerlin, J. 2004. "Placement of Piezoelectric Laminate Actuator for Active Structural Acoustic Control," In: *International Conference on Noise & Vibration Engineering, ISMA 2004*, Leuven, Bélgica, pp. 41–54.

Charon, W. 1997. "Practical Design and Verification of LQG Controllers as Applied to Active Structure," *Journal of Intelligent Material Systems and Structures*, 8(11):960–985.

Clark, R.L., Saunders, W.R. and Gibbs, G.P. 1998. *Adaptive Structures: Dynamics and Control*, John Wiley & Sons, Inc., New York, USA.

Folcher, J.P. and El Ghaoui, L. 1994. "State-Feedback Design via Linear Matrix Inequalities: Application to a Benchmark Problem," IEEE ISBN 0-7803-1872-2, pp. 1217–1222.

Gahinet, P., Nemirovski, A., Laub, A.J. and Chiliali, M. 1995. "LMI Control Toolbox User's Guide," The Mathworks Inc., Natick, MA, USA.

Gawronski, W. 1998. *Dynamics and Control of Structures: A Modal Approach*, 1st edn, p. 231, Springer-Verlag, New York.

Geromel, J.C. 1989. "Convex Analysis and Global Optimization of Joint Actuator Location and Control Problems," *IEEE Transactions on Automatic Control*, 34(7):711–720.

Geromel, J.C., Peres, P.L.D. and Bernussou, J. 1991. "On a Convex Parameter Space Method for Linear Control Design of Uncertain Systems," *SIAM J. Control and Optimization*, 29(2):381–402.

Ghaoui, L., Oustry, F. and AitRami, M. 1997. "A Cone Complementary Linearization Algorithm for Static Output-Feedback and Related Problems," *IEEE Transactions on Automatic Control*, 42(8):1171–1176.

Gonçalves, P.J.P., Lopes, Jr., V. and Assunção, E. 2002. "H_2 and H_∞ Norm Control of Intelligent Structures using LMI Techniques," In: *Proceeding of ISMA 26 – International Conference on Noise and Vibration Engineering*, Leuven, Belgium.

Gonçalves, P.J.P., Silva, S., Turra, A.E. and Lopes, Jr., V. 2003a. "Active Vibration Control in Smart Structures Comparing the Control Algorithms: IMSC and LMI," In: *Proceeding of X DINAME – Symposium on Dynamic Problems of Mechanics*, Ubatuba SP, Brazil, pp. 171–176.

Gonçalves, P.J.P., Lopes, Jr., V. and Brennan, M.J. 2003b. "Using LMI Techniques To Control Intelligent Structures," In: *XXI IMAC – Conference on Structural Dynamics*, Kissimmee, Florida.

Grigoriadis, K.M. and Skelton, R.E. 1996. "Low-Order Control Design for LMI Problems using Alternating Projection Methods," *Automatica*, 32(8):1117–1125.

Halim, D. and Moheimani, S.O.R. 2003. "An Optimization Approach to Optimal Placement of Collocated Piezoelectric Actuators and Sensor on a Thin Plate," *Mechatronics*, 13(1):February 2003, 27–47.

Juang, J. and Minh, Q.P. 2001. *Identification and Control of Mechanical System*, Cambridge University Press, ISBN 0521783550.

Kabamba, P.T., Meerkov, S.M. and Poh, E.K. 1994. "H_2 Optimal Zeros," *IEEE Transactions Automatic Control*, 39(6):1298–1301.

Lopes, V. Jr., Pereira, J.A. and Inman, D.J. 2000. "Structural FRF Acquisition via Electric Impedance Measurement Applied to Damage Detection," In: *XVIII – IMAC*, São Antonio, TX, USA, pp. 1549–1555.

Lopes, Jr., V., Steffen, Jr., V. and Inman, D.J. 2004. "Optimal Placement of Piezoelectric Sensor/Actuator for Smart Structures Vibration Control," In: Udwadia, F.E., Weber, H.I. and Leitmann, G. (eds), *Dynamical Systems and Control*, pp. 221–236, Chapman and Hall/CRC, Boca Raton.

Meirovitch, L. 1990. *Dynamics and Control of Structures*, John Wiley & Sons, New York, USA. ISBN 0-471-62858-1.

Oliveira, M.C. and Geromel, J.C. 2000. "Linear Output Feedback Controller with Joint Selection of Sensors and Actuators," *IEEE Transactions on Automatic Control*, 45(12):2412–2419.

Peres, P.L.D. 1997. "Controle H_2 e H_∞: Caracterização por Desigualdades Matriciais Lineares," Tese de Livre Docência (in Portuguese), Universidade Estadual de Campinas, UNICAMP, Campinas, SP.

Sana, S. and Rao, V. 2000. "Application of Linear Matrix Inequalities in the Control of Smart Structural Systems," *Journal of Intelligent Material and Structures*, 11(4):311–323.

Yan, Y.J. and Yam, L.H. 2002. "A Synthetic Analysis on Design of Optimum Control for an Optimized Intelligent Structure," *Journal of Sound and Vibration*, 249(4):775–784.